Electrochimica Acta 154 (2015) 456–461

Contents lists available at ScienceDirect

Electrochimica Acta

journal homepage: www.elsevier.com/locate/electacta

A conductivity study of preferential solvation of lithium ion in acetonitrile-dimethyl sulfoxide mixtures

Nataliia Mozhzhukhina [a], M. Paula Longinotti [a,*], Horacio R. Corti [a,b], Ernesto J. Calvo [a]

[a] Instituto de Química Física de los Materiales, Medio Ambiente y Energía (INQUIMAE-CONICET), Facultad de Ciencias Exactas y Naturales, Universidad de Buenos Aires, Pabellón II, Ciudad Universitaria, (1428), Buenos Aires, Argentina
[b] Departamento de Física de la Materia Condensada, Comisión Nacional de Energía Atómica, Avda. General Paz 1499 (1650), San Martín, Buenos Aires, Argentina

ARTICLE INFO

Article history:
Received 16 October 2014
Received in revised form 28 November 2014
Accepted 4 December 2014
Available online 6 December 2014

Keywords:
Electrical conductivity
solvation
redox potential
ACN–DMSO mixtures
lithium

ABSTRACT

The electrical mobility of $LiPF_6$ in acetonitrile–dimethyl sulfoxide (ACN–DMSO) mixtures, a potential electrolyte in oxygen cathodes of lithium-air batteries, has been studied using a very precise conductance technique, which allowed the determination of the infinite dilution molar conductivity and association constant of the salt in the whole composition range. In the search for preferential Li^+ ion solvation, we also measured the electrical conductivity of tetrabutylammonium hexafluorophosphate ($TBAPF_6$), a salt formed by a bulky cation, over the same composition range. The results show a qualitative change in the curvature of the $LiPF_6$ molar conductivity composition dependence for ACN molar fraction (x_{ACN}) ~ 0.95, which was not observed for $TBAPF_6$. The dependence of the measured Li/Li^+ couple potential with solvent composition also showed a pronounced change around the same composition. We suggest that these observations can be explained by Li^+ ion preferential solvation by DMSO in ACN–DMSO mixtures with very low molar fractions of DMSO.

1. Introduction

Li-ion batteries have conquered the market of portable electronics after their successful commercialization by Sony in the early 1990s. However, in recent years numerous efforts have been performed in order to meet a global energy challenge and develop Li-based batteries that would possess a superior power density to that of Li-ion, such as Li-S or Li-air [1]. Li-air batteries are theoretically very promising and this technology has recently gained a wide scientific attention with an increasing number of investigations conducted each year [2–4].

Among the research concerning the potentially interesting electrolytes for lithium batteries, transport studies are of great interest and importance. Numerous studies of transport properties of several electrolyte systems for Li-ion batteries are nowadays available [5–7]. However, it has been shown that typical electrolyte systems employed in Li-ion batteries (based on organic carbonates and ethers) are not appropriate for Li-air batteries due to the electrolyte decomposition by the oxygen reduction reaction (ORR) intermediates and/or products [8–16]. Thus, more information on transport properties in other electrolyte systems for Li-air batteries is needed. Recent studies have suggested that dimethyl sulfoxide (DMSO) seems to be a promising candidate for Li-air batteries [17–19]. Using Infrared spectroscopy, we failed to detect dimethyl sulfone in the electrolyte resulting from the nucleophilic attack by the electrogenerated superoxide radical anion [20]. However, there is a controversy on the stability of DMSO in contact with Li_2O_2 [21,22]. Sharon *et al.* [21] pointed out that DMSO may not be a suitable solvent for rechargeable $Li-O_2$ cells due to its oxidation by reactive oxygen species and lithium oxides. McCloskey *et al.* [23] have shown that the balance of oxygen consumed in the ORR and that evolved in the oxygen evolution reaction (OER) during charging is always less than 0.9 due to the heterogeneous chemical reaction of the solid peroxide with the electrolyte or the carbon cathode. However, DMSO exhibits unusual properties related to the ORR that is stabilization of the intermediate O_2^- anion, which does not occur in other solvents [18]. We have reported [24], that soluble superoxide radical anions can be detected at a rotating ring disk electrode (RRDE) system in lithium solutions of acetonitrile (ACN) containing 0.1 M DMSO (x_{ACN} = 0.995), while no evidences of soluble O_2^- are observed in lithium acetonitrile solutions. We have suggested that those observations could be due to the preferential solvation of Li^+ cation by DMSO molecules that in turn prevents the disproportion of lithium superoxide ($2\,O_2Li \rightarrow Li_2O_2 + O_2$). In order to test this hypothesis, in this work, we have studied the ionic conductivity of lithium hexafluorophosphate ($LiPF_6$) in comparison to

* Corresponding author.
E-mail address: longinot@qi.fcen.uba.ar (M. P. Longinotti).

http://dx.doi.org/10.1016/j.electacta.2014.12.022
0013-4686/

tetrabutylamonium hexafluorophosphate ($TBAPF_6$) in ACN–DMSO mixtures in the whole composition range. These results were complemented with measurements of Li/Li^+ electrode potential as a function of the composition of the ACN–DMSO mixture.

2. Experimental

2.1. Materials

Anhydrous dimethyl sulfoxide (DMSO) ≥99.9% (SIGMA–ALDRICH), acetonitrile (ACN) (SIGMA–ALDRICH), tetrabutylammonium hexafluorophosphate ($TBAPF_6$) for electrochemical analysis, ≥99.0% (FLUKA), and lithium hexafluorophosphate ($LiPF_6$) battery grade ≥99.99% trace metals basis (ALDRICH), were stored in an argon-filled MBRAUN glove box with oxygen content ≤0.1 ppm and water content <2 ppm. DMSO and ACN were dried for several days over molecular sieves 3A (SIGMA–ALDRICH); $TBAPF_6$ and $LiPF_6$ were used as received. All solutions were prepared inside the glove box and the water content was measured using Karl Fisher coulometric titration (831 KFCoulometer (Metrohm)). All solutions were found to contain less than 20 ppm of water at the beginning and less than 30 ppm of water at the end of conductivity measurements.

2.2. Redox potential of the Li/Li^+ electrode in DMSO/ACN mixtures.

The anode material for the Li-air battery is lithium metal; therefore it is common to refer to the Li/Li^+ scale when presenting electrochemical studies of the cathode reaction (oxygen reduction reaction ORR and oxygen evolution reaction OER). However, Li metal itself is rarely used as a reference electrode, but typically other non-aqueous reference electrodes are used, which are referred to Li/Li^+ by measuring its potential versus lithium wire or calibrating with ferrocene couple. However, while referring an electrode to the lithium wire, it should be taken into account that the potential of the Li/Li^+ couple depends on the electrolyte in which it measured since Li^+ solvation energy depends notably on the solvent.

In this work, we studied the Li/Li^+ potential dependence on solvent composition in ACN–DMSO mixtures by resorting to the cell:

$Li_2Mn_2O_4/LiMn_2O_4$/1 M $LiPF_6$ (DMSO)//0.1 M $LiPF_6$ (ACN–DMSO)/Li

The reference $Li_2Mn_2O_4/LiMn_2O_4$ electrode was prepared as described:

1) $LiMn_2O_4$ synthesis: Li_2CO_3 and MnO_2 were mixed in a molar relation 0.51:2, grounded, pressed and heated at 350 °C for 12 h and at 800 °C for 24 h.
2) $Li_2Mn_2O_4$ synthesis: equimolar amounts of $LiMn_2O_4$ and LiI were mixed and placed in a vacuum oven at 80 °C overnight.
3) Equimolar quantities of $LiMn_2O_4$ and $Li_2Mn_2O_4$ were mixed with Carbon black (10% of total mixture weight) and PVDF binder (10% of total mixture weight) and dissolved in an appropriate organic solvent to make an ink.
4) A Pt wire was covered with the ink, and placed in a fritted glass compartment containing 1 M $LiPF_6$ in DMSO solution.

All measurements were performed inside the glove box.

The liquid junction potential between the 1 M $LiPF_6$ (DMSO) solution and the 0.1 M $LiPF_6$ solution in the studied ACN–DMSO mixture was calculated as:

$$E_j = (t_+ - t_-)\frac{RT}{F}\ln\left(\frac{a_1}{a_2}\right) \quad (1)$$

where t_+ and t_- are the transport numbers of the cation and anion, respectively and a_1 and a_2 the activities of the salt that form the liquid junction. We approximated the electrolytes activities with the concentration of the salt solutions considering this correction is minor. Based on conductivity studies [25–31], the transport numbers of Li^+ in ACN and DMSO are 0.39 and 0.36, respectively. The calculated liquid junction potential varies between 0.013 V in ACN, and 0.017 V in DMSO and can be neglected over all the range of ACN–DMSO compositions.

It should also be considered that the $Li_2Mn_2O_4/LiMn_2O_4$ reversible reference electrode is immersed in DMSO, while the Li/Li^+ electrode is in the ACN–DMSO mixture. Thus, an additional potential difference exists on the interface of DMSO with the corresponding ACN–DMSO mixture, due to the variation in the dielectric constant of the mixtures. In order to correct the measured potential due to the interface between the DMSO reference electrode and the ACN–DMSO mixture, we have also calibrated the $Li_2Mn_2O_4/LiMn_2O_4$ reference electrode with the ferrocene $Fe(C_5H_5)_2$ – ferrocenium couple for all the solutions of interest. The calibration was performed by measuring cyclic voltammograms in 0.1 M $LiPF_6$ + 5–10 mmol $Fe(C_5H_5)_2$ in ACN–DMSO solutions, using a standard 3-electrode electrochemical cell with a Pt working electrode, a $Li_2Mn_2O_4/LiMn_2O_4$ reference electrode and a carbon rod counter electrode.

2.3. Viscosity of ACN–DMSO mixtures.

Owing to the significant difference between the literature reported viscosity values of the mixtures [32,33] (up to 20% difference for some compositions), we measured the viscosities of ACN–DMSO mixtures in the whole composition range with Cannon–Fenske (Ostwald modification) viscometers size 25 (0.5–2 mPa s) and size 50 (0.8–4 mPa s), calibrated with water.

For viscosity determinations, viscometers were filled with the solution of interest inside the glovebox, sealed with Teflon caps, taken out of the glove box and thermostated in a water bath at 298.15 ± 0.05 K. Then, the viscometers were opened and measurements were performed immediately to avoid water contamination.

2.4. Conductivity of $LiPF_6$ and $TBAPF_6$ in ACN–DMSO mixtures.

An air-tight glass conductivity cell with a mixing bulb and platinized platinum electrodes was used to determine the conductivity of $LiPF_6$ and $TBAPF_6$ in ACN–DMSO mixtures as a function of electrolyte concentration ($10^{-5} - 10^{-3}$ M) and solvent composition. Conductivity measurements for $LiPF_6$ were performed for ACN–DMSO mixtures with ACN molar fractions (x_{ACN}) = 0.000, 0.192, 0.373, 0.453, 0.586, 0.697, 0.798, 0.898, 0.947, 0.968, 0.995, and 1.000. Measurements for $TBAPF_6$ were performed for x_{ACN} = 0.269, 0.492, 0.754, and 0.960.

The cell constant, $k_{cell} = 0.0710 \pm 0.0008\ cm^{-1}$ at 298.15 K, was determined using a standard KCl aqueous solution of known specific conductivity [34].

The conductivity measurements were performed according to the following protocol: first, the conductivity cell was filled with the solvent inside the glove box, by weighting the corresponding amounts of ACN and DMSO to obtain the desired composition. Then, the cell was transferred to an oil bath thermostatized at 298.15 ± 0.08 K and after reaching thermal equilibrium, the solvent resistance was measured. Afterwards, increasing weighted amounts of a stock solution of $LiPF_6$ or $TBAPF_6$, prepared inside the glove box, in an ACN–DMSO mixture of equal composition, were added. Additions were transferred from a stock solution containing vessel to the conductivity cell (both air-tight and equipped with septum) with the use of a syringe. The resulting solution was homogenized by manual stirring; after reaching a new thermal equilibrium, the solution resistance was determined.

Table 1
Molar conductivity of $LiPF_6$ and $TBAPF_6$ in ACN–DMSO mixtures and thermophysical properties of the corresponding mixtures.

x_{ACN}	δ (g/cm^3)	ε	η (mPa s)	Λ° $LiPF_6$ (S cm^2 mol^{-1})
0.000	1.096	46.7	1.990	34.1 ± 0.3
0.192	1.043	43.9	1.437	46.0 ± 0.1
0.373	0.9901	42.1	1.023	64.3 ± 0.3
0.453	0.9657	41.4	0.8760	70.23 ± 0.06
0.586	0.9238	40.3	0.6788	89.1 ± 0.5
0.697	0.8868	39.4	0.5517	100.7 ± 0.3
0.798	0.8521	38.5	0.4626	109.3 ± 0.6
0.898	0.8158	37.3	0.3934	137.4 ± 0.4
0.947	0.7977	36.7	0.3659	145.4 ± 0.3
0.968	0.7896	36.4	0.3550	155.5 ± 0.5
0.995	0.7796	36.1	0.3426	165 ± 2
1.000	0.7775	36.0	0.3401	173.2 ± 0.7

x_{ACN}	δ (g/cm^3)	ε	η (mPa s)	Λ° $TBAPF_6$ (S cm^2 mol^{-1})
0.000	1.096	46.7	1.990	33.6 ± 1.4*
0.269	1.021	43.1	1.2476	52.0 ± 0.6
0.492	0.9538	41.1	0.8131	75.2 ± 0.3
0.754	0.8674	38.9	0.4992	114.6 ± 0.2
0.960	0.7929	36.6	0.3594	156.5 ± 0.5
1.000	0.7775	36.0	0.3401	164.8 ± 0.1*

* data obtained from λ_i values reported in Ref. [25,27,28]

The salt molar conductivities, Λ, were determined according to

$$\Lambda = \frac{\kappa}{c} = \left(\frac{1}{R} - \frac{1}{R_0}\right)\frac{k_{cell}}{c} \quad (2)$$

where κ is the solution specific conductivity, c is the electrolyte molar concentration, R is the solution resistance, and R_0 is the solvent resistance.

For the resistance measurements a Precise LCR meter (G^{W}INSTEK) was used. An AC voltage (100 mV) was applied to the electrodes at different frequencies and the resistive and capacitive components were recorded, considering an equivalent resistance–capacitance parallel circuit. The resistance was recorded at several frequencies between 0.3 and 5 kHz and the extrapolated value at infinite frequency was computed.

3. Conductivity data treatment

The salt molar conductivity data as a function of concentration was analyzed with the equation given by Fuoss–Hsia–Fernandez Prini (FHFP) [27], which accounts for ionic association:

$$\Lambda(c) = \Lambda^0 - S(\alpha c)^{\frac{1}{2}} + E\alpha c.\ln(\alpha c) + J_1(d)\alpha c - J_2(d)(\alpha c)^{\frac{3}{2}} - K_a\Lambda\gamma_{\pm}^{\ 2}(\alpha c) \quad (3)$$

where c is the salt molar concentration, d the distance of closest approach of the free ions, whose concentration is αc, with α the degree of dissociation. The constants S, E, J_1 and J_2 were calculated using the equations given by Fernandez Prini [27] with the viscosity and dielectric constant data of the ACN–DMSO mixtures. The mean activity coefficient of the ions was approximated by the Debye–Hückel equation:

$$\ln\gamma_{\pm} = \frac{-A\sqrt{\alpha c}}{1 + d\kappa} \quad (4)$$

where κ is the reciprocal radius of the ionic atmosphere, and A was calculated using the dielectric constant data of the mixtures.

The degree of dissociation α is related to the association constant K_a by

$$K_\alpha = \frac{(1-\alpha)}{\gamma_{\pm}^2\alpha^2 c} \quad (5)$$

A non linear fit of Λ, c data allowed the determination of Λ° and K_a.

The salt molar concentration c was determined from the weights of salt and solvents using the density of the mixture. The thermophysical properties of the ACN–DMSO mixtures (density [32] and dielectric constant [33]) at 298.15 K were fitted with polynomial equations as a function of composition, and the corresponding values for the measured compositions are given in Table 1. Viscosity was fitted in logarithmic scale as a function of composition as will be discussed in Section 4.2.

4. Results and discussion

4.1. Redox potential of the Li/Li$^+$ electrode in ACN–DMSO mixtures.

Fig. 1 shows the Li/Li$^+$ electrode potential *vs.* the reversible lithium electrode in ACN–DMSO mixtures in the whole composition range. Corrections, due to the potential difference in the inferface between the DMSO reference electrode and the DMSO-ACN solution, determined by measuring the $Li_2Mn_2O_4/LiMn_2O_4$

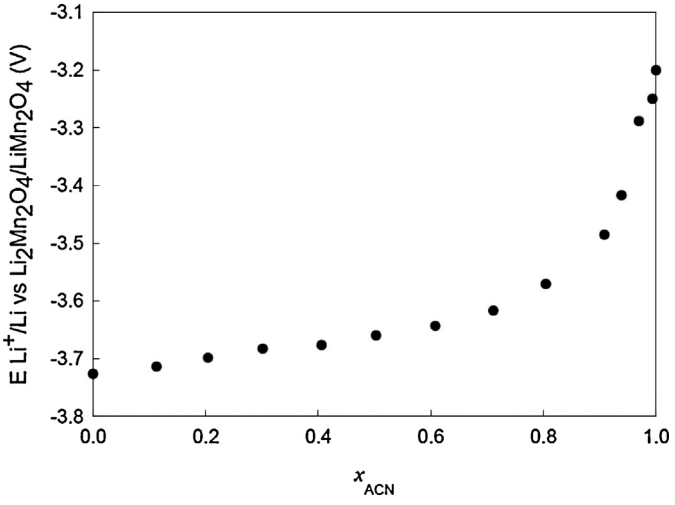

Fig. 1. Li/Li$^+$ electrode potential *vs.* Li$^+$ reversible electrode as a function of ACN molar fraction in ACN–DMSO mixtures.

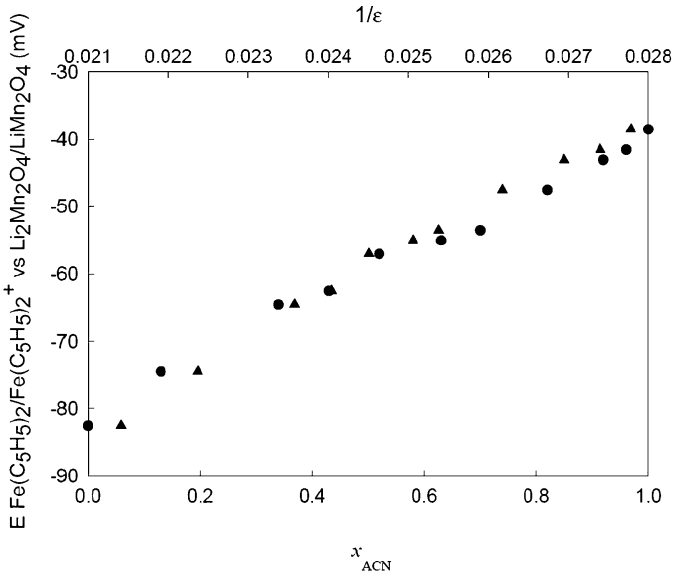

Fig. 2. Redox potential of the ferrocene-ferrocenium couple versus $Li_2Mn_2O_4$/$LiMn_2O_4$ reversible reference electrode, determined in solutions of 0.1 M $LiPF_6$, 5–10 mM ferrocene, as a function of x_{ACN} bottom scale (●), and as a function of inverse dielectric constant top scale (▲).

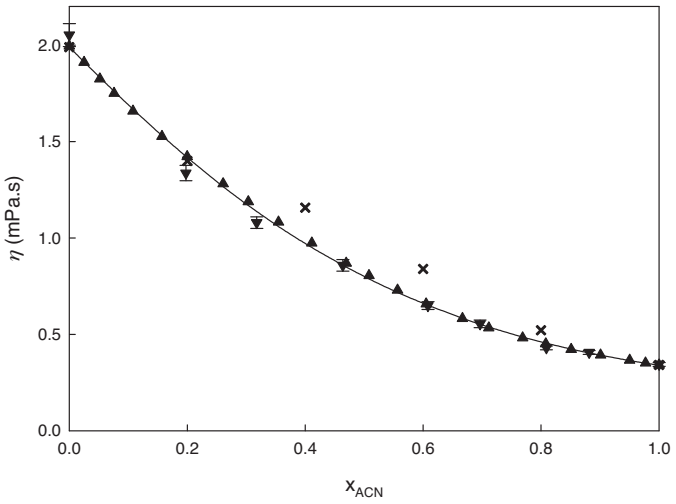

Fig. 3. Viscosity of ACN–DMSO mixtures as a function of ACN molar fraction. Data reported by Gill *et al.* [32] (X), Grande *et al.* [33] (▲), and that measured in this work (▼). The bold line corresponds to the polynomial fit performed in this work.

reference electrode *vs.* the ferrocene – ferrocenium couple, plotted in Fig. 2, were taken into account in the calculations.

As it was previously pointed out in a recent work [20], the potential of the Li/Li^+ couple (*vs.* $Li_2Mn_2O_4/LiMn_2O_4$ reference electrode) depends strongly on the electrolyte used to measure it. This is due to the fact that lithium solvation free energy depends notably on the solvent, for instance, the potential of a non-aqueous Ag/Ag^+ reference electrode *vs.* Li/Li^+ (0.1 M $LiPF_6$) varies from 3.23 V in ACN to 3.70 V in DMSO.

In Fig. 1, it can be observed that around $x_{ACN} \sim 0.8$ the potential of the Li/Li^+ electrode increases markedly, while around $x_{ACN} \sim 0.95$ the curvature of the potential composition dependence seems to vary. This seems to indicate that an important solvation effect is observed in ACN–DMSO mixtures with small DMSO contents. In order to further test this hypothesis, we studied the conductivity of $LiPF_6$ and $TBAPF_6$ in the whole composition range to compare the molar conductivity of the solvated Li^+ ion with that of the bulky non solvated TBA^+ cation (Section 4.3).

4.2. Viscosity of ACN–DMSO mixtures.

Fig. 3 shows our viscosity measurements in comparison with reported data by other authors [32,33]. As it can be observed, our measurements agree, within the experimental error (between 2.3 and 3.6%), with viscosity data reported by Grande *et al.* [33] Thus, in order to fit the experimental viscosity data as a function of composition, we chose as input values our experimental data and that reported by these authors.

4.3. Conductivity of $LiPF_6$ and $TBAPF_6$ in ACN–DMSO mixtures.

Table 1 and Fig. 4 show the molar conductivities of $LiPF_6$ and $TBAPF_6$, at infinite dilution, as a function of composition. Thermophysical properties (density, dielectric constant, and viscosity) of the corresponding mixtures, calculated as previously described, are included in Table 1.

In order to estimate the uncertainty in the molar conductivity of the salt, at each concentration and solvent composition, we should analyze the uncertainties in the salt molarity, temperature, and solvent conductivity (background conductivity).

The salt molar concentration was determined by weight, using the calculated density of the mixtures with an uncertainty of ±1%. The temperature of the sample was determined with an uncertantity of ±0.08 °C, and considering that the molar conductivity of the salts changes approximately 2%/K, the uncertainty in the temperature introduces an uncertainty of 0.16% in the measured conductivity. Finally, it was estimated that the change of water sorbed by the solvent mixture during the measurements (≈10 ppm) has a negligible effect on the measured conductivity, because the solvent conductivity (before adding the salt) does not change significantly.

Therefore, it can be concluded that the relative error of the molar conductivity should not exceed 1.2%. The cell constant was determined with an error of 1.1%, but this does not affect the precision, but the accuracy of the conductivity measurements.

The errors assigned to the values of Λ° in Table 1, obtained from the standard deviation of the fits of $\Lambda(c)$ *vs.* c with Eq. (3), vary between 0.09% and 1.2% for our calculations. Figure S1 in the Supplementary Information show, as mode of example, the deviations of the experimental data to the calculated best fit for the conductivity measurements of $LiPF_6$ in the pure solvents.

Reported data [25–31] for the ionic infinite molar conductivities of Li^+ and PF_6^- ions in ACN [25–27], and DMSO [25,28–31], indicate that for $LiPF_6$, $\Lambda^\circ = 173.1 \pm 0.3\ S\,cm^2\,mol^{-1}$ in pure ACN, and $\Lambda^\circ = 33 \pm 2\ S\,cm^2\,mol^{-1}$ in pure DMSO, being our measurements in excellent agreement with these results.

As expected, the infinite dilution molar conductivities of both salts increase with increasing ACN content, since the viscosity decreases with increasing ACN content in the mixture. However, while Λ° for $TBAPF_6$ in ACN–DMSO mixtures exhibits a monotonic concentration dependence, which could be properly fitted with a cubic equation all over the composition range, Λ° for $LiPF_6$ exhibits a non-monotonic composition dependence with a clear change in the curvature around $x_{ACN} \sim 0.95$.

The association constants of $LiPF_6$ are only significant in pure ACN ($K_a = 43 \pm 7$) and for the mixture with $x_{ACN} = 0.995$ ($K_a = 28 \pm 16$). This result can be explained considering that the dielectric constant of the mixtures increases with increasing DMSO content (see Table 1). The infinite dilution molar conductivities of $TBAPF_6$ in the pure solvents were extracted from ionic molar conductivity data [25,27,28] of the component ions. The ionic association for TBAPF6 in ACN–DMSO solutions mixtures for $x_{ACN} = 0.27$, 0.49, 0.75 and 0.96 are negligible and the salt is fully dissociated in this concentration range.

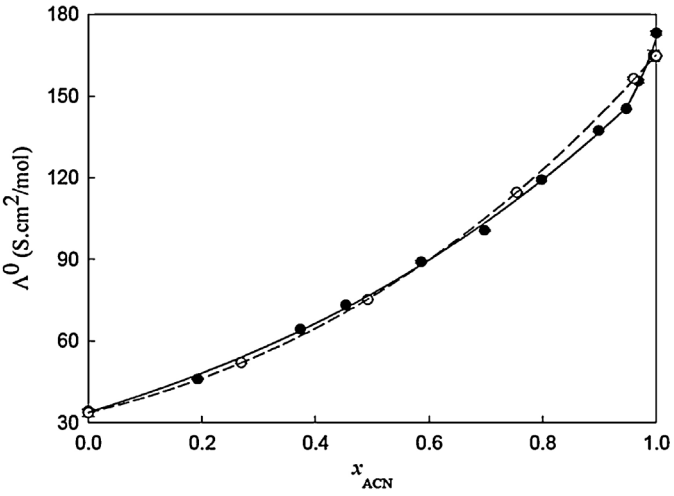

Fig. 4. Infinite dilution molar conductivity values for $LiPF_6$ (●) and $TBAPF_6$ (○) in ACN–DMSO mixtures as a function of ACN molar fraction. Λ° for $TBAPF_6$ in the pure solvents were taken from Ref [25,27,28]. Error bars for the conductivities plotted in this figure are smaller than the size of the symbols. The dashed line corresponds to the polynomial fit performed for $TBAPF_6$ as a function of composition, while the solid lines, merging at $x_{ACN} \sim 0.95$, are the best fits for $LiPF_6$.

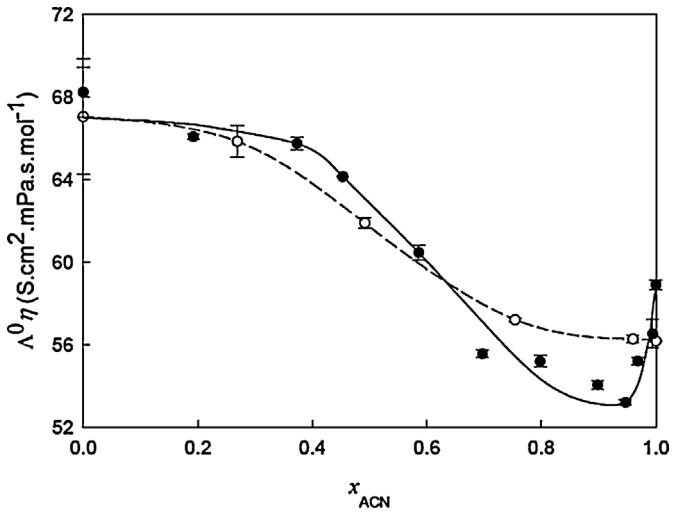

Fig. 5. Walden product for the limiting molar conductivities of $LiPF_6$ (●) and $TBAPF_6$ (○) in ACN–DMSO mixtures as a function of ACN molar fraction. The dotted and bold lines for $TBAPF_6$ and $LiPF_6$, respectively, were added as a guide to the eye.

The viscosity of the ACN–DMSO mixtures changes from 0.34 mPa s in pure ACN to 1.99 mPa s in pure DMSO. Thus, the viscous friction is primarily responsible for the strong ionic mobility changes with composition. In order to eliminate the effect of viscosity in the conductivity composition dependence we plotted, in Fig. 5, for $LiPF_6$ and $TBAPF_6$, the Walden product, expressed by,

$$\Lambda^0\eta = \frac{z^2eF}{Ar} \tag{6}$$

where ($z = z_+ = |z_-|$), e is the electron charge, F is the Faraday constant, ($1/r = 1/r+ + 1/r-$) is the sum of the reciprocal hydrodynamic radii of the ions, and A is a constant whose value depends on the friction conditions (6π for stick and 4π for slip boundary conditions, respectively).

In this figure it can be observed that the Walden product for $TBAPF_6$ is not constant as predicted by the Walden rule, but decreases from 67 S cm^2 mPa s mol^{-1} in DMSO down to 56 S cm^2 mPa s mol^{-1} in ACN. This implies an apparent change in the radius of the salt. However, this is not plausible taking into account that the ions are bulky and should behave essentially as non-solvated ions. Therefore, the composition dependence of the Walden product needs to be analyzed in terms of a more complete model that includes the dielectric friction of the ions with the solvent dipoles [35–37]. Briefly, the coupling of the ion mobility with the dipole solvent relaxation time leads to an expression for the local viscosity near the ion given by [37],

$$\eta(r) = \eta_0\left(1 + \frac{R_{HO}^4}{r^4}\right) \tag{7}$$

where R_{HO} is the Hubbard–Onsager radius, given by:

$$R_{HO} = \frac{\tau e^2(\varepsilon_0 - \varepsilon_\infty)}{16\pi\eta_0\varepsilon_0} \tag{8}$$

with ε_0 and ε_∞ being the static and infinite frequency dielectric constants of the solvent, and τ the dielectric relaxation time. The values of R_{HO} are 0.175 nm for DMSO and 0.183 nm for ACN at 298.15 K [25], indicating that the relation $\eta(r)/\eta_0$ is lower for DMSO as compared with ACN, in agreement with the trend observed in Fig. 5, where the Walden product decreases from DMSO to ACN.

For $LiPF_6$, the Walden product exhibits a minimum, not observed for $TBAPF_6$, for $x_{ACN} \sim 0.95$. If we hypothesize that the dielectric friction effect for TBA^+ is similar to that for Li^+, the reduction in the Walden product for $LiPF_6$ observed when decreasing the ACN content when going from $x_{ACN} = 1$ to $x_{ACN} = 0.95$ can be interpreted as an increment in the value of r. Considering, that PF_6^- behaves essentially as a non solvated ion, this increment can be considered fundamentally as an increment in the Li^+ hydrodynamic radius. This can be hypothesized to be due to the fact that for $x_{ACN} = 0.95$ the first solvation shell of the Li^+ ion, which is formed by ACN molecules in pure ACN, is partially or totally replaced by the larger DMSO molecules. Computer simulation results [38] reinforce this hypothesis showing that lithium ion first solvation shell is formed exclusively by DMSO molecules for $x_{ACN} < 0.9$, while incorporates ACN molecules above this composition. Computer simulation results indicate that notable changes in lithium solvation are produced for very small quantities of DMSO in ACN–DMSO mixtures in accordance with our measurements. Thus, although the two solvents exhibit "similar" physicochemical properties, such as their dipolar moment and aprotic character, changes in lithium solvation are produced for very small DMSO contents in the mixtures.

5. Conclusions

In this work we conclude, by redox potential of the Li/Li^+ electrode and electrical conductivity of $LiPF_6$ and $TBAPF_6$ measurements in ACN–DMSO mixtures, that lithium ion is preferentially solvated by DMSO even for very small molar fractions of DMSO in ACN.

This preferential solvation effect is of great importance since it stabilizes the superoxide ion preventing the disproportion of lithium superoxide ($2\,O_2Li \rightarrow Li_2O_2 + O_2$) [24].

Our finding is very relevant for the optimization of the electrolytes for Li-air batteries, since it could help to find an adequate DMSO–ACN solvent composition which prevents the disproportion of lithium superoxide, minimizing DMSO oxidation by reactive oxygen species and lithium oxides, while having high conductivity values.

Acknowledgments

We thank financial support from CONICET (PIP 095), ANPCyT-FONCyT (PICT 2012 N° 1452) and University of Buenos Aires (UBACyT 20020100100519). MPL, HRC and EJC are members of CONICET.

Appendix A. Supplementary data

Supplementary data associated with this article can be found, in the online version, at http://dx.doi.org/10.1016/j.electacta.2014.12.022.

References

[1] P.G. Bruce, S.A. Freunberger, L.J. Hardwick, J.M. Tarascon, Li-O_2 and Li-S batteries with high energy storage, Nature Mater. 11 (2012) 19–29.
[2] J. Christensen, P. Albertus, R.S. Sanchez-Carrera, T. Lohmann, B. Kozinsky, R. Liedtke, J. Ahmed, A. Kojic, A critical review of Li/Air batteries, Electrochem. Soc. 159 (2012) R1–R30.
[3] G. Girishkumar, B. McCloskey, A.C. Luntz, S. Swanson, W. Wilcke, Lithium-air battery: promise and challenges, J. Phys. Chem. Lett. 1 (2010) 2193–2203.
[4] K.M. Abraham, Lithium-Air and other batteries beyond lithium-ion batteries, Lithium Batteries, John Wiley & Sons, Inc, 2013, pp. 161–190.
[5] K. Xu, Nonaqueous liquid electrolytes for lithium-based rechargeable batteries, Chem. Rev. 104 (2004) 4303–4417.
[6] H.B. Han, S.S. Zhou, D.K. Zhang, S.W. Feng, F.F. Li, K. Lui, W.F. Feng, J. Nie, H. Li, X.J. Huang, M. Armand, Z.B. Zhou, Lithium bis(fluorosulfonyl) imide (LiFSI) as conducting salt for nonaqueous liquid electrolytes for lithium-ion batteries: Physicochemical and electrochemical properties, J. Power Sources 196 (2011) 3623–3632.

[7] H. Hang, J. Guo, D. Zhang, S. Feng, W. Feng, J. Nie, Z. Zhuo, Lithium (fluorosulfonyl)(nonaqueousfluorobutanesulfonyl) imide (LiFNFSI) as conducting salt to improve the high temperature resilence of lithium-ion cells, Electrochem. Commun. 113 (2011) 265–268.
[8] S.A. Freunberger, Y. Chen, N.E. Drewett, J.L. Hardwick, F. Bardé, P.G. Bruce, The lithium-oxygen battery with ether-based electrolytes, Angew. Chem. Int. Ed. Engl. 50 (2011) 8609–8613.
[9] S.A. Freunberger, Y. Chen, Z. Peng, J.M. Griffin, L.J. Hardwick, F. Bardé, P. Novák, G. Bruce, Reactions in the rechargeable lithium-O_2 battery with alkyl carbonate electrolytes, J. Am. Chem. Soc. 133 (2011) 8040–8047.
[10] B.D. McCloskey, B.S. Bethune, R.M. Shelby, G. Girishkumar, A.C. Luntz, Solvents critical role in nonaqueous lithium-oxygen battery electrochemistry, J. Phys. Chem. Lett. 2 (2011) 1161–1166.
[11] Z. Peng, S.A. Freunberger, L.J. Hardwick, Y. Chen, V. Giordani, F. Bardé, P. Novák, D. Graham, J.M. Tarascon, P.G. Bruce, Oxygen reactions in non-aqueous Li^+ electrolyte, Angew. Chem. Int. Ed. Engl. 50 (2011) 6351–6355.
[12] H. Wang, K. Xie, Investigation of oxygen reduction chemistry in ether and carbonate based electrolytes for Li-O_2 batteries, Electrochim. Acta 64 (2012) 29–34.
[13] W. Xu, J. Hu, M.H. Enhelhard, S.A. Towne, J.S. Hardy, J. Xiao, J. Feng, M.H. Hu, J. Zhang, F. Ding, M.E. Gross, J.G. Zhang, The stability of organic solvents and carbon electrode in nonaqueous Li-O_2 batteries, J. Power Sources 215 (2012) 240–247.
[14] W. Xu, K. Xu, V.V. Viswanathan, S.A. Towne, J.S. Hardy, J. Xiao, Z. Nie, D. Hu, D. Wang, J.G. Zhang, Reaction mechanisms for the limited reversibility of Li-O_2 chemistry in organic carbonate electrolytes, J. Power Sources 196 (2011) 9631–9639.
[15] R. Younesi, M. Hahlin, K. Edstrom, Surface characterization of the carbon cathode and the lithium anode of Li-O_2 batteries using $LiClO_4$ or LiBOB salts, Acs Appl. Mater. Interf. 5 (2013) 1333–1341.
[16] C.J. Barile, A.A. Gewirth, Investigating the Li-O_2 battery in an ether based electrolyte using differential electrochemical mass spectrometry, J. Electrochem. Soc. 160 (2013) A549–A552.
[17] Z. Peng, S.A. Freunberger, Y. Chen, P.G.A. Bruce, A reversible and higher-rate Li-O_2 battery, Science 337 (2012) 563–566.
[18] M.J. Trahan, M. Sanjeev, E.J. Plichta, M.A. Hendrickson, K.M. Abraham, Studies of lithium-air cells utilizing dimethyl dulfoxide-based electrolyte, J. Electrochem. Soc. 160 (2013) A259–A267.
[19] D. Xu, Z.L. Wang, J.J. Xu, L.L. Zhang, X.B. Zhang, Novel DMSO-based electrolyte for high performance rechargeable Li-O_2 batteries, Chem. Commun. 48 (2012) 6948–6950.
[20] N. Mozhzhukhina, L.P. Méndez De Leo, E.J. Calvo, Infrared spectroscopy studies on stability of dimethyl sulfoxide for application in a Li–air battery, J. Phys. Chem. C 117 (2013) 18375–18380.
[21] D. Sharon, M. Afri, M. Noked, A. Garsuch, A.A. Frimer, D. Aurbach, Oxidation of dimethyl sulfoxide solutions by electrochemical reduction of oxygen, J. Phys. Chem. Lett. 4 (2013) 3115–3119.
[22] D.G. Kwabi, T.P. Batcho, C.V. Amanchukwu, N. Ortiz-Vitoriano, P. Hammond, C.V. Thompson, Y. Shao-Horn, Chemical instability of dimethyl sulfoxide in lithium-air batteries, J. Phys. Chem. Lett. 5 (2014) 2850–2856.
[23] B.D. McCloskey, A. Valery, A.C. Luntz, S.R. Gowda, G.M. Wallraff, J.M. Garcia, T. Mori, L.E. Krupp, Combining accurate O_2 and Li_2O_2 assays to separate discharge and charge stability limitations in non-aqueous Li-O_2 batteries, J. Phys. Chem. Lett. 4 (2013) 2989–2993.
[24] E.J. Calvo, N. Mozhzhukhina, A rotating ring disk electrode study of the oxygen reduction reaction in lithium containing non aqueous electrolyte, Electrochem. Commun. 31 (2013) 56–58.
[25] D.L. Goldfarb, M.P. Longinotti, H.R. Corti, Electrical conductances of tetrabutlyammonium and decamethylferrocenium hexafluorophosphate in organic solvents, J. Solution Chem. 30 (2001) 307–322.
[26] J. Barthel, L. Iberl, J. Rossmaier, H.J. Gores, B. Kaukal, Conductance of 1,1-electrolytes in acetonitrile solutions from −40° to 35°C, J. Solution Chem. 19 (1990) 321–337.
[27] R. Fernandez Prini, M. Spiro, Conductance and transference numbers in organic solvents, in: A.K. Covingston, T. Dickinson (Eds.), Physical Chemistry of Organic Sovents Systems, Part 3, Chapter 5, Plenum Press, New York, 1973.
[28] N.G. Tsierkezos, A.I. Philippopoulos, Studies of ion solvation and ion association of n-tetrabutylammonium hexafluorophosphate and n-tetrabutylammonium tetraphenylborate in various solvents, Fluid Phase Eq. 277 (2009) 20–28.
[29] M.N. Roy, P. Chandra, A. Chakraborti, Conductivity is a contrivance to explore ion-pair and triple-ion structure of ethanoates in tetrahydrofuran dimethyl sulfoxide and their binaries, Fluid Phase Eq. 322–323 (2012) 159–166.
[30] J.H. Exner, E.C. Steiner, Solvation and ion pairing of alkali-metal alkoxides in dimethyl sulfoxide. Conductimetric studies, J. Am. Chem. Soc. 96 (1974) 1782–1787.
[31] M.D. Archer, R.P.H. Grasser, Electrolyte solutions in dimethyl-sulfoxide. Part 2-Caesium iodide, Trans. Faraday Soc. 62 (1966) 3451–3458.
[32] D.S. Gill, D.S. Rana, S.P. Jauhar, Transport studies of some 1:1 copper(I) perchlorate complexes in acetonitrile-dimethylsulphoxide mixtures, Zeits. Phys. Chem. 225 (2011) 69–77.
[33] M.C. Grande, M. García, C.M. Marschoff, Density and viscosity of anhydrous mixtures of dimethylsulfoxide with acetonitrile in the range (298.15 to 318.15) K, J. Chem.Eng. Data 54 (2009) 652–658.
[34] Y.C. Wu, W.K. Koch, W.J. Hamer, R.L. Kay, Review of electrolytic conductance standards, J.Solution Chem. 16 (1987) 985–997.
[35] R. Zwanzig, Dielectric friction on a moving ion. II. Revised theory, J. Chem. Phys. 52 (1970) 3625–3628.
[36] J. Hubbard, L. Onsager, Dielectric dispersion and dilectric friction in electrolyte solutions, J. Chem. Phys. 67 (1977) 4850–4857.
[37] P.G. Wolynes, Dynamics of electrolyte solutions, Annu. Rev. Phys. Chem. 31 (1980) 345–376.
[38] R. Semino, G. Zaldívar, E.J. Calvo, D. Laria, Lithium solvation in dimethyl sulfoxide–acetonitrile mixtures, J. Chem. Phys 141 (2014) 214509.